Pergamon

Ocean Engineering 29 (2002) 1463–1477

OCEAN ENGINEERING

www.elsevier.com/locate/oceaneng

Analysis of Wells turbine design parameters by numerical simulation of the OWC performance

A. Brito-Melo, L.M.C. Gato *, A.J.N.A. Sarmento

Mechanical Engineering Department, Instituto Superior Técnico, Technical University of Lisbon, Av. Rovisco Pais, 1049-001 Lisbon, Portugal

Received 22 May 2001; accepted 30 August 2001

Abstract

This paper investigates by numerical simulation the influence of the Wells turbine aerodynamic design on the overall plant performance, as affected by the turbine peak efficiency and the range of flow rates within which the turbine can operate efficiently. The problem of matching the turbine to an oscillating water column (OWC) is illustrated by taking the wave climate and the OWC of the Azores power converter. The study was performed using a time-domain mathematical model based on linear water wave theory and on model experiments in a wave tank. Results are presented of numerical simulations considering several aerodynamic designs of the Wells turbine, with and without guide vanes, and with the use of a bypass pressure-relief valve. © 2002 Elsevier Science Ltd. All rights reserved.

Keywords: Wave energy; Oscillating water column; Equipment; Wells turbine

1. Introduction

The Wells turbine has been the most commonly adopted solution to the air-to-electricity energy conversion problem in oscillating water column (OWC) wave energy converters. These essentially consist of a capture pneumatic chamber, open at the bottom front to the incident wave, a turbine and an electrical generator. The incident wave motion excites the oscillation of the internal free surface of the entrained water mass in the pneumatic chamber, which produces a low-pressure reci-

* Corresponding author. Tel.: +351-21-841-7411; fax: +351-21-841-7398.
E-mail address: lgato@hidro1.ist.utl.pt (L.M.C. Gato).

0029-8018/02/$ - see front matter © 2002 Elsevier Science Ltd. All rights reserved.
PII: S0029-8018(01)00099-3

procating flow that drives the turbine. A few full-scale turbine prototypes have been built and installed in grid-connected power plants in European countries, e.g. the 500 kW Wells monoplane turbine with guide vanes installed in the Island of Pico, Azores (Falcão, 2000), and 2×250 kW biplane contrarotating turbine of the LIMPET plant, at Islay, Scotland (Heath et al., 2000).

The greatest challenges to designers of equipment for wave energy converters are the intrinsically oscillating nature and the random distribution of the wave energy resource. These features are absent or much less severe in other competing energy technologies. The air turbine in an OWC converter is subject to flow conditions (randomly reciprocating flow), which, with respect to efficiency, are much more demanding than in turbines in almost any other application. The Wells turbine, while reaching only a moderately high peak efficiency as compared with conventional turbines, can operate in reciprocating flow without the need of a rectifying valve system. The turbine, on the one hand, is required to extract energy from air whose flow rate, in each of the two directions, oscillates between zero and a maximum value, which in turn has an extremely large variation from wave to wave and with sea conditions. On the other hand, at fixed rotational speed, turbines in general, and Wells turbines in particular, are capable of operating with good efficiency only within a limited range of flow conditions around the peak efficiency point. The power output of Wells turbines is known to be low (or even negative) at small flow rates (the flow rate passes through zero twice in a wave cycle) and it drops sharply for flow rates above a critical value due to aerodynamic losses produced by rotor blade stalling. Therefore, the turbine is expected to perform poorly in very energetic sea-states or whenever violent wave peaks occur. Mounting a bypass pressure-relief valve on the top of the air chamber as proposed in the Azores plant may prevent this problem. The valve is controlled to limit the maximum pressure and suction in the chamber (depending on the turbine rotational speed) to prevent the instantaneous air flow rate through the turbine from exceeding the values above which aerodynamic stalling at the rotor blades would produce a severe fall in power output. Numerical simulations (Brito-Melo et al., 1996; Falcão and Justino, 1999) indicate that a reduction in turbine size and a substantial increase in the annual production of electrical energy might be achieved by the use of a bypass pressure-relief valve. Moreover, recent studies (theoretical and model testing) indicate that blade sections especially designed for Wells turbine rotors can significantly enlarge the range of flow rates within which the turbine operates efficiently and reduce aerodynamic losses under partially stalled flow conditions, in comparison with other blade designs which give a higher peak efficiency within a narrower range of flow rates through the turbine. This raises the question of whether, in view of the total annual produced electrical energy and taking into account the hydrodynamic performance of the OWC device, it is more appropriate to select a turbine aerodynamic design which allows an enlarged range of flow rates at which the turbine operates efficiently or whether it is better to adopt a turbine design which gives a higher peak efficiency value with a reduced range of flow rates at which the turbine operates efficiently. Furthermore, it is of interest to know to what extent this issue might be dependent on the use of a pressure-relief valve.

The main objective of the present work is to investigate the influence of the Wells turbine aerodynamic design on the overall plant performance, as affected by the turbine peak efficiency and the range of flow rates within which the turbine can operate efficiently. Realistic characteristics are assumed for the turbine and the use of a bypass pressure-relief valve is also considered. Since the resulting pressure changes in the chamber are dependent on the turbine characteristics and the pressure-relief valve influences the turbine operation, the hydrodynamic process of energy extraction is also modified. The hydrodynamics of the conversion of wave energy into pneumatic energy is predicted by using a time-domain mathematical model based on linear water wave theory and on model experiments in a wave tank as described in Sarmento and Brito-Melo (1996). The conversion of pneumatic energy into electrical energy is predicted by a suitable computational model of the power take-off equipment based on the results extrapolated from aerodynamic tests on a scale-model and on empirical approximations for the generator losses (Brito-Melo et al., 1996). This paper presents the results of numerical simulations considering several aerodynamic designs of the Wells turbine, with and without guide vanes, and the use of the pressure-relief valve. The problem of matching the turbine to an OWC is illustrated by taking the wave climate and the OWC of the Azores wave power converter.

2. Wave-to-wire model

2.1. Plant operation

The wave-to-wire model concerns the operation of an OWC equipped with a Wells turbine, a bypass valve of unlimited capacity and a variable speed turbo-generator, under a set of representative sea-state conditions.

The Wells turbine is known to exhibit an approximately linear relationship between the turbine pressure drop $p(t)$ and the flow rate $q_t(t)$. Then we may write the turbine characteristic as $K = p(t)/q_t(t) = p_s(\Omega)/q_s(\Omega)$, where $p_s(\Omega)$, and $q_s(\Omega)$ are maximum values of pressure and flow rate (prior to the onset of aerodynamic stall at the turbine rotor blades), which (for a given turbine) depend on the turbine rotational speed Ω. The use of a properly controlled bypass pressure-relief valve prevents the occurrence of stall at the turbine rotor blades. The valve is controlled to ensure that $|p(t)| \leq p_s(\Omega)$. Then $|q_s(t)| \leq q_s(\Omega)$. The excess flow rate $q_v(t)$ passes through the valve to (or from) the atmosphere.

The inertia of the rotating parts is assumed large enough so that rotational speed Ω may be considered approximately constant over the time-intervals simulating a given sea-state (about 15 minutes). This allows Ω to be optimized for each representative record of the sea-state, in order to maximize the electrical energy production. The turbine rotational speed is allowed to vary between the synchronous speed of the generator and twice its value. Summing the product of the time-averaged electrical power output with the occurrence frequency for all data records gives the overall annual average electrical power output.

2.2. Hydrodynamic model

The hydrodynamic model is based on the pressure model presented in Sarmento and Falcão (1985). According to the OWC performance description presented in Section 2.1, the mass balance across a control surface enclosing the pneumatic chamber is given by

$$\frac{p(t)}{K} + q_v(t) = q(t) - \frac{V_0}{\gamma P_a}\frac{\mathrm{d}p(t)}{\mathrm{d}t} \tag{1}$$

where $q(t)$ is the volume flow rate displaced by the free-surface inside the chamber, V_0 denotes the volume of the air in the chamber under undisturbed conditions, P_a is the atmospheric pressure and γ is the ratio of specific heats. As stated in Section 2.1, $q_v(t) = 0$ if $|p(t)| < p_s(\Omega)$ (i.e. when the valve is not operating). According to the linear water wave theory, the volume flow rate displaced by the free-surface inside the chamber may be decomposed as $q(t) = q_d(t) + q_r(t)$, where $q_d(t)$ is the diffraction flow rate, due to incident wave action assuming the internal and the external free-surfaces at constant atmospheric pressure, and $q_r(t)$ is the radiation flow rate due only to the pressure oscillation $p(t)$ in otherwise calm waters. Under the assumptions of the linearized wave theory, we may apply the convolution theorem to obtain the solution of a linear problem in terms of an impulse response (Pipes and Harvill, 1970), as follows:

$$q_r(t) = \int_{-\infty}^{t} h_r(t-\tau)p'(\tau)\,\mathrm{d}\tau \tag{2}$$

where $p'(\tau)$ is the time-derivative of the pressure inside the chamber and τ represents a time-lag. The upper limit of the integral in Eq. (2) represents the present instant t because the process is causal (Cummins, 1962). The impulse response function $h_r(t)$ can be obtained from the hydrodynamic coefficients of the OWC computed with a numerical model, such as the WAMIT (Lee et al., 1996) or the AQUADYN-OWC (Brito-Melo et al., 1999), or by tank testing. Here we use an estimate of the impulse response function obtained in free-oscillation transient experiments from 1:35 scale testing of the Azores OWC wave power plant (see Sarmento and Brito-Melo, 1996, for details).

Time series for the diffraction flow, $q_d(t)$, have also been obtained in energy extraction experiments with the scaled model subject to a set of 44 sea-states representative of the Azores power plant site. In these experiments a device producing an equivalent air pressure drop simulated the turbine. The flow rate $q_t(t)$ could be obtained as a function of $p(t)$ from the device calibration curve. The diffraction flow time-series for each of the 44 sea-states was estimated by solving Eq. (1) (with $q_v(t) = 0$) using the pressure records from the energy extraction experiments, and the experimental estimate of $h_r(t)$ previously obtained in the transient experiments.

2.3. Power take-off equipment

The power take-off sub-model is based on results extrapolated from small-scale turbine tests (Gato et al., 1996; Webster and Gato, 1999a,b) and on empirical data for the turbine and generator losses (Brito-Melo et al., 1996). The average power at the turbine shaft for a period T is given by

$$W_s = \frac{\Omega}{T}\int_0^T [L(\Omega,q_t(t)) - L_m(\Omega)]\,dt \tag{3}$$

where L is the aerodynamically produced turbine-torque and L_m the torque due to mechanical losses (especially bearing losses). For stall-free conditions, L is approximated by a second-order polynomial. In order to provide the necessary performance data to study the matching of the power take-off equipment and the pneumatic chamber, the data from small-scale turbine tests are modified using a simple mean-line turbine flow analysis method to take into account the rotor solidity S and the hub-to-tip ratio. Ignoring the postponement of stall when the Reynolds number is increased, scale effects are taken into account by correcting the torque curve of the turbine model. This is done multiplying (dividing) the positive (negative) values of L by $f = 0.8/0.706$. This corrects the torque curve of the unswept NACA 0015 bladed rotor with guide-vanes to match a peak efficiency of $\eta_{max} = 0.80$. For the preliminary design of the turbine a maximum blade tip speed of 160 ms^{-1} is assumed. The average electrical power output is obtained by subtracting the generator losses from the average power at the turbine shaft. The model for the generator losses includes the Joule losses, the iron losses, the ventilation losses and the mechanical losses (Brito-Melo et al., 1996).

3. Results and discussion

Experimental research on different types of rotor blades has been conducted recently to improve the aerodynamic performance of the Wells turbine (Raghunathan, 1995; Gato et al., 1996; Curran and Gato, 1997; Webster and Gato, 1999a,b). Among these types, we consider two turbine blade configurations, which may give a wider range of flow rates within which the turbine can operate with fairly good efficiency, in comparison with that of the more standard NACA 0015 unswept bladed turbine rotor: they are the backward-swept NACA 0015 blades (Webster and Gato, 1999a), Fig. 1, and the optimized HSIM-15-262123-1576 unswept blades (Gato and Henriques, 1996), Fig. 2. For comparison we take results for the NACA 0015 unswept blades (Gato et al., 1996).

Figs. 3 and 4 show experimental results from unidirectional-flow small-scale testing at the IST rig (Webster and Gato, 1999a,b). Results presented in Figs. 3 and 4 refer to high-solidity Wells turbine rotors (rotor outer radius $R = 0.295$ m, constant chord $c = 125$ mm, rotor solidity $S = 0.64$, equipped with the blades referred to

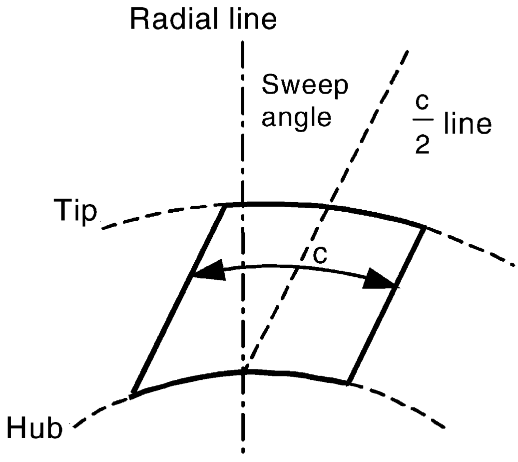

Fig. 1. Rotor blade sweep angle.

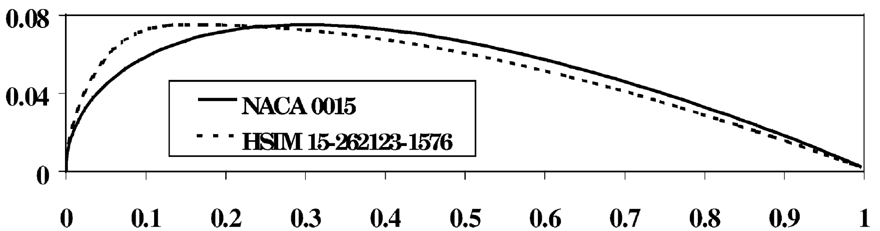

Fig. 2. The NACA 0015 and HSIM 15-262123-1576 sections.

above, with and without guide vanes. The figures show, in dimensionless form, experimental results for the efficiency $\eta = L\Omega/(q_t p)$, pressure drop $p^* = p/(\rho\Omega^2R^2)$, and torque $L^* = L/(\rho\Omega^2R^5)$ as functions of the flow rate coefficient U* (ρ is the air density). Results in Fig. 3 for the turbines without guide vanes show that the NACA 0015 unswept rotor has $\eta_{\max} = 0.583$ at $U^* = 0.114$, and stalls at $U^* = 0.21$. The NACA 0015 30° backward-swept rotor has a lower $\eta_{\max} = 0.583$, with a lower flow rate for the onset of stall, $U^* = 0.17$, but without exhibiting the sharp decrease in the torque that occurs in the unswept rotor. Furthermore, under stall conditions, the torque of the swept rotor becomes negative at a much higher flow rate, $U^* > 0.45$, whereas for the unswept blades the efficiency becomes negative for $U^* > 0.3$. The unswept HSIM bladed rotor shows a $\eta_{\max}$ similar to that of the backward-swept rotor, but produces a soft progressive stall of the flow through the rotor blades, with notably higher efficiency for a wide range of flow rates after the onset of stall.

Fig. 4 shows a corresponding plot for the same turbine rotors when equipped with a double row of guide vanes. The experimental results plotted in Fig. 4 show that the use of guide vanes increases $\eta_{\max}$ for any of the above geometries, i.e. from 0.583 to 0.706, 0.551 to 0.613 and 0.553 to 0.669, for the NACA 0015 unswept and

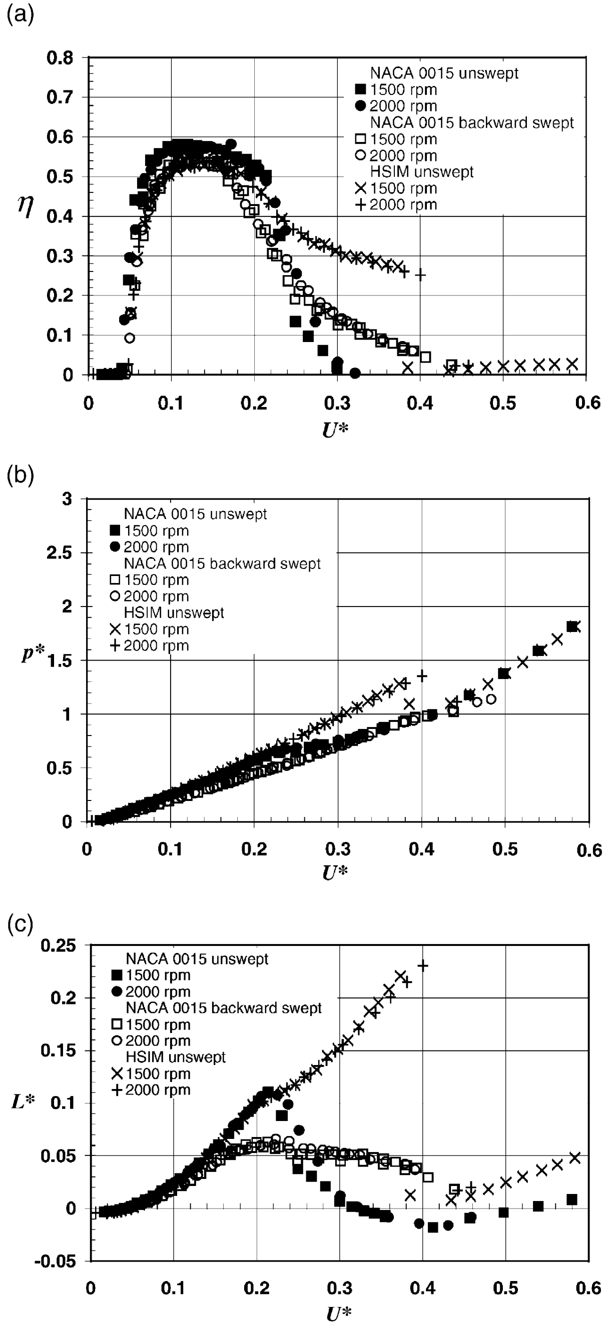

Fig. 3. Unswept and 30° backward-swept NACA 0015 and unswept HSIM bladed rotor turbines, without guide vanes: measured values of efficiency (a), pressure drop (b) and torque (c) against flow rate coefficient.

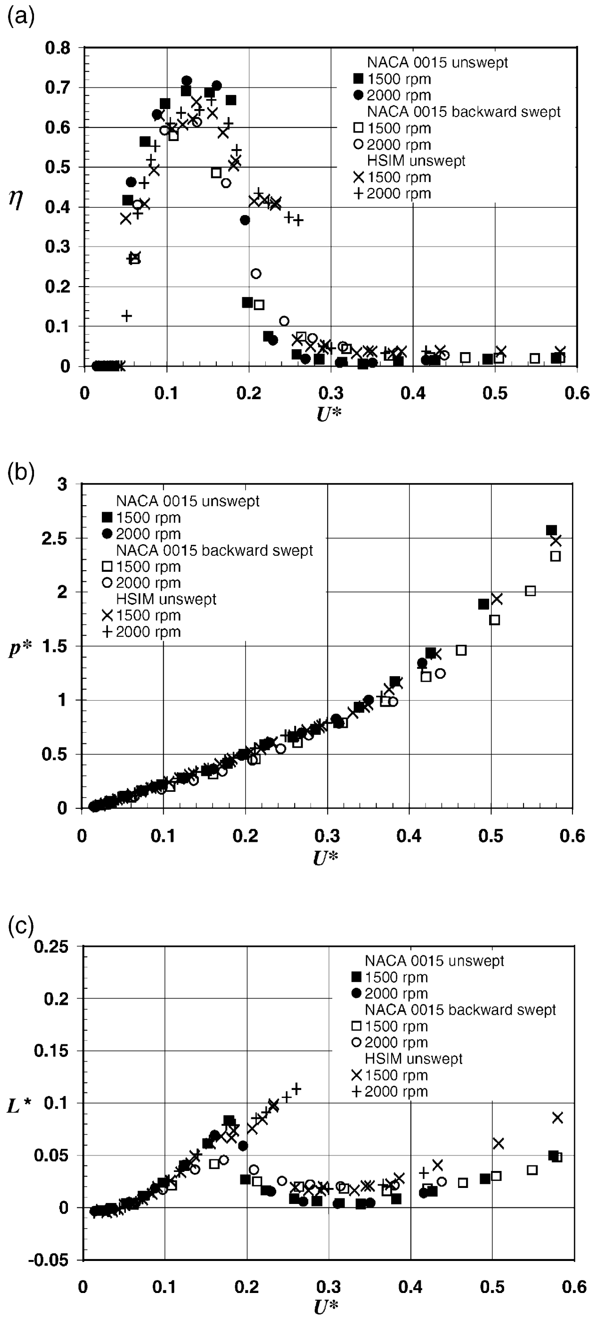

Fig. 4. Unswept and 30° backward-swept NACA 0015 and unswept HSIM bladed rotor turbines, with guide vanes: measured values of efficiency (a), pressure drop (b) and torque (c) against flow rate coefficient.

backward-swept rotors and the HSIM unswept rotor, respectively. Furthermore, we find that the use of guide vanes narrows the range of flow rates within which the turbine works with positive torque.

Table 1 summarizes the performance data for the six turbines, where U_a^* and U_b^* are the minimum and maximum flow rate coefficients respectively, at which the efficiency is nominally $\eta = 0.5\eta_{max}$. Therefore, $\Phi = U_a^*/U_b^*$ and $\Delta = U_a^* - U_b^*$ give an indication of the operational range while $(\Delta p_0^*/U^*)_{\eta = \eta_{max}}$ is the pressure–flow ratio in the approximately rectilinear region. In the above performance comparison, constant overall solidity was assumed for the different turbine configurations. Results in Table 1 show that the rotor blade geometry has a remarkable influence on the turbine performance. In particular, some rotor geometries give a considerable wider range of flow rates within which the turbine operates efficiently, in comparison with others that have higher peak efficiency within a narrower range of flow rates.

Figs. 5–7 plot the average electrical power output as given by the numerical simulation for the set of the 44 representative records of the wave climate for the Azores Plant site, taking into account the frequency of occurrence of each sea-state. The results give the turbine characteristic K for several values of the rated power $W_0 = p_s q_s$. Table 2 indicates the values of the flow coefficient U_s^* at which the different types of turbine rotor were designed and the bypass pressure-relief valve is actuated.

3.1. NACA 0015 unswept bladed rotor with and without guide vanes

Fig. 5 presents the results of the numerical simulation to study the effect of the use of guide vanes with the NACA 0015 unswept bladed rotor. Fig. 5 shows that the use of guide vanes provides a significant increase in the average electrical power output, both with and without the presence of the bypass pressure-relief valve. The curves plotted in Figs. 3 and 4 for the unswept NACA 0015 rotor, with and without guide vanes, respectively, show that the turbine with guide vanes has $\eta_{max} \approx 0.72$

Table 1
Peak efficiency, useful flow rate range and damping ratio for several turbine models (overall solidity *S*=0.64)

Turbine rotor	With guide vanes			Without guide vanes		
	NACA 0015 unswept	NACA 0015 swept-back	HSIM unswept	NACA 0015 unswept	NACA 0015 swept-back	HSIM unswept
η_{max}	0.706	0.613	0.669	0.583	0.551	0.553
$(U^*)_{\eta = \eta_{max}}$	0.124	0.137	0.154	0.114	0.129	0.131
U_a^*	0.050	0.062	0.057	0.051	0.058	0.059
U_b^*	0.197	0.209	0.275	0.251	0.232	0.360
Φ	0.254	0.297	0.207	0.203	0.250	0.164
Δ	0.147	0.147	0.218	0.200	0.174	0.301
$(\Delta p_0^*/U^*)_{\eta = \eta_{max}}$	2.19	1.87	2.38	2.54	2.04	2.79

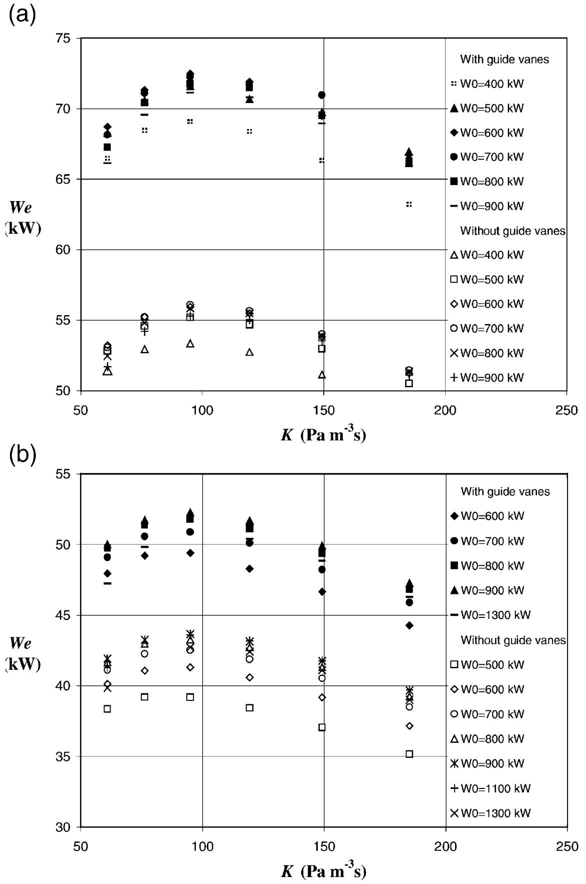

Fig. 5. Unswept NACA 0015 bladed rotor turbine with and without guide vanes working (a) with and (b) without the bypass valve: average electrical power conversion as a function of the turbine characteristic *K*, for several values of the turbine-rated power.

whereas for the turbine without guide vanes $\eta_{max} < 0.60$. Nevertheless, the torque curve for the turbine without guide vanes exhibits a wider range of flow rates over which the turbine performs with good efficiency. The results of the numerical simulations reveal the usefulness of the guide vanes. In addition, they show that, under the above conditions, the aerodynamic design criterion for the turbine should be to maximize the turbine peak efficiency even if that may result in a narrower curve of efficiency versus flow rate. Furthermore, it may be found that the use of guide vanes leads to a small increase in the turbine size, which, however, should not constitute a significant penalty since the turbine cost is only a small fraction of the overall plant cost.

Results in Fig. 5a also show that the trend for the electrical power output as a function of the turbine-rated power is the same regardless of whether guide vanes are considered or not. A significant increase in the electrical power output is seen

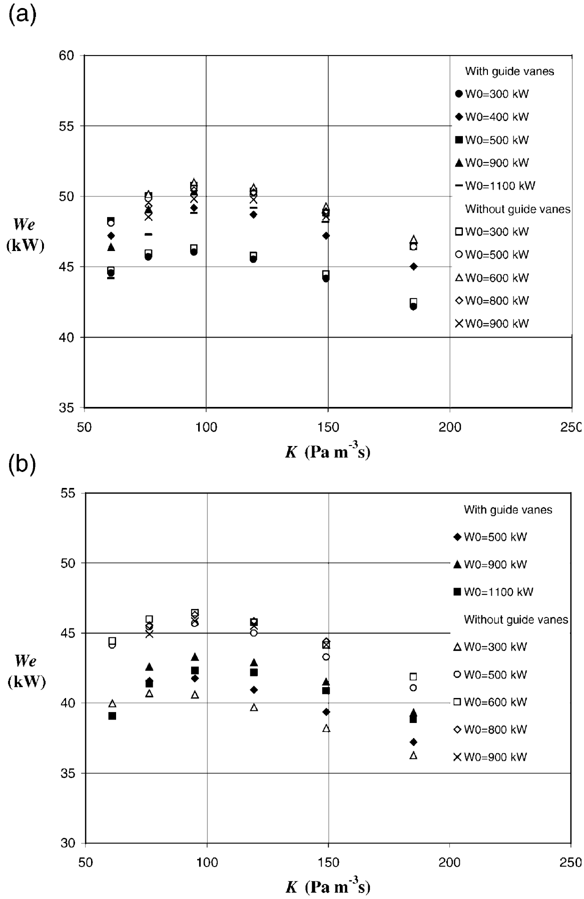

Fig. 6. 30° backward-swept NACA 0015 bladed rotor turbine with and without guide vanes working (a) with and (b) without the bypass valve: average electrical power conversion as a function of the turbine characteristic *K*, for several values of the turbine-rated power.

to occur as the turbine-rated power increases up to 600 kW. Maximum electrical power output is achieved for a turbine characteristic $95<K<119.4$ Pa m^{-3} s, within the range of turbine-rated powers considered in the simulations.

Fig. 5b presents the results of the numerical simulation in the absence of a bypass relief valve. Under such conditions, the total converted power is considerably smaller, in comparison with the corresponding cases when a bypass relief valve is present. Furthermore, the converted electrical power increases with turbine-rated power up to 900 kW. Above this value, the converted power decreases due to the turbine losses at small flow rates and the increase in the electrical and mechanical losses. Maximum converted power is obtained for a value of the constant *K* similar to that obtained using the bypass relief valve.

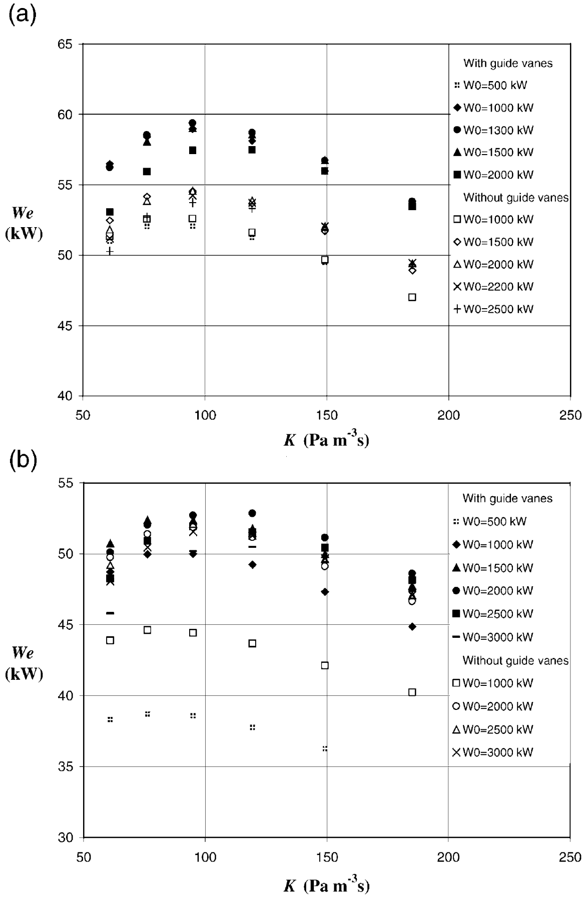

Fig. 7. HSIM bladed rotor turbine with and without guide vanes working (a) with and (b) without the bypass valve: average electrical power conversion as a function of the turbine characteristic K, for several values of the turbine-rated power.

Table 2
Design value of the flow coefficient for which the bypass valve is actuated

Turbine rotor	U_s^*	
	With guide vanes	Without guide vanes
NACA 0015 unswept	0.176	0.213
NACA 0015 swept	0.170	0.178
HSIM unswept	0.275	0.38

3.2. NACA 0015 swept bladed rotor, with and without guide vanes

Fig. 6 presents the results of the numerical simulation to study the effect of the use of guide vanes with the NACA 0015 30° backward-swept bladed rotor. It can be seen that the use of guide vanes is not beneficial in the absence of the relief valve. This is due to the poorest performance of the guide vane equipped turbine under stalled flow conditions, as compared with the turbine without guide vanes (see Figs. 3 and 4).

The comparison between Figs. 5 and 6 shows that the performance of the swept bladed rotor is poorer than that of the unswept bladed rotor, assuming that guide vanes and a pressure-relief valve are used. This result agrees with the performance curves shown in Fig. 4 for the same turbines.

The performance comparison of the backward-swept NACA 0015 bladed rotor with that of the unswept NACA 0015 rotor, both without guide vanes and considering the use of a relief valve, shows that the backward-swept rotor blades produce less energy in comparison with that from the corresponding unswept bladed rotor. In these conditions, the advantage of the unswept rotor arises from its higher efficiency prior to stall, in comparison with that of the backward-swept blades. However, a small benefit is obtained with the backward-swept blades if no bypass pressure-relief valve is present and no guide vanes are use.

For a given turbine-rated power, the electrical energy conversion as a function of the turbine characteristic K is similar for both turbine types, i.e. maximum conversion is obtained when $95<K<119.4$ Pa m^{-3} s, regardless of the use or not of the bypass relief valve.

Furthermore, it can be seen that the use of the bypass valve in conjunction with the backward-swept bladed rotor does not lead to a significant increase in the mean power conversion, in contrast with what was found for the corresponding conditions in the case of the unswept bladed turbine. This is due to the wider range of flow rates within which the backward-swept bladed rotor turbine can operate with fairly good efficiency.

3.3. HSIM bladed rotor with and without guide vanes

Results presented in Fig. 7 compare the performance of the unswept HSIM bladed rotor with and without guide vanes in the presence (Fig. 7a) or absence (Fig. 7b) of a bypass valve. It can be seen that the electrical energy produced is slightly higher when the bypass pressure-relief valve operates with the turbine without guide vanes. In the case of a turbine with guide vanes, it may be found that a more substantial increase in the electrical power conversion is obtained by using a bypass pressure-relief valve.

When comparing the HSIM bladed rotor with the NACA 0015 (Fig. 5), in both cases without guide vanes and with a bypass valve, we observe that better performance is obtained from the turbine with the NACA 0015 bladed rotor. This means that the higher-peaked narrower efficiency curve of the NACA 0015 bladed rotor should be preferred to the lower wider curve for the HSIM bladed rotor.

Fig. 4 shows that the torque curve of the unswept NACA 0015 bladed rotor is more beneficial than that of the HSIM bladed rotor when a bypass valve is present. The opposite is true if no bypass valve is present. Although the HSIM bladed rotor has positive torque over a wider range of flow rates than the NACA bladed rotor, with and without guide vanes, the results show that this is not a benefit if the pressure-relief valve is used, at least for the wave climate at the Azores plant.

If the bypass valve is not considered then a slightly better performance can be achieved using the HSIM blades. We note that the HSIM blades lead to higher rated power and smaller turbines, which, however, may not be an advantage if the costs of the electrical generator and its power electronics are taken into account.

4. Conclusion

A computational model that simulates the power conversion chain from the wave-to-wire was used to match several Wells turbine designs to an OWC wave energy converter. A main concern was the Wells turbine's peak efficiency versus the (inherent limited) width of the range of flow rates within which the turbine can operate efficiently, especially if this is considered in conjunction with the use of a bypass pressure-relief valve in an OWC plant.

The bypass pressure-relief valve was found to provide higher levels of electrical energy production for each of turbine designs studied under similar working conditions. This increase is more significant for the unswept NACA 0015 bladed rotor with guide vanes. This turbine gives the best power conversion among all the turbine configurations studied.

The poorest performance is provided by the unswept NACA 0015 bladed rotor without guide vanes and without the bypass pressure-relief valve. The mathematical model predicts for this case a maximum average electrical power production that is only about 60% of what can be achieved with the best arrangement, i.e. the unswept NACA 0015 bladed rotor with guide vanes working in parallel with a pressure-relief valve.

When the relief valve is not considered, the unswept HSIM bladed rotor gives the best power conversion, with or without guide vanes.

The use of the bypass pressure-relief valve was found to provide a reduction in the turbine size and rated power.

When the bypass pressure-relief valve is used in the control of an OWC, then the turbine design should aim at maximizing the turbine peak efficiency even if that results in a narrower efficiency curve. Conversely, when the bypass valve is not considered, the numerical results showed that the turbine aerodynamic design should lead to a turbine capable of operating with fairly good efficiency over a wide range of flow rates.

Acknowledgements

The work reported here was partly financially supported by Program PRAXIS XXI under contract BD/5148/95 and by IDMEC and MARETEC, Lisbon.

References

Brito-Melo, A., Sarmento, A.J.N.A., Gato, L.M.C., 1996. Mathematical extrapolation of tank testing results: application to the Azores wave pilot plant. In: Proceedings of the Second European Wave Power Conference. European Commission, pp. 141–147.

Brito-Melo, A., Sarmento, A.J.N.A., Clement, A.H., Delhommeau, G., 1999. A 3D boundary element code for the analysis of OWC wave power plants. In: Proceedings of the Ninth International Offshore and Polar Engineering Conference, Brest, ISOPE, I., pp. 188–195.

Cummins, W.E., 1962. The impulse response function and ship motions. Schiffstechnick 9, 101–109.

Curran, R., Gato, L.M.C., 1997. The energy conversion performance of several types of Wells turbine designs. Proceedings of the Institution of Mechanical Engineers, Part A 211 (A2), 133–145.

Falcão, A.F. de O., 2000. The shoreline OWC wave power plant at the Azores. In: Proceedings of the Fourth European Wave Power Conference, Energy Centre Denmark, Danish Technological Institute, Tastrup, 42–48, Denmark, paper B1.

Falcão, A.F. de O., Justino, P.A.P., 1999. OWC wave energy devices with air-flow control. Ocean Engineering 26, 1249–1273.

Gato, L.M.C., Henriques, J.C.C., 1996. Optimization of symmetrical profiles for Wells turbine rotor blades. In: Proceedings of the ASME Fluids Engineering Division Summer Meeting, FED-238(3), pp. 623–630.

Gato, L.M.C., Warfield, V., Thakker, A., 1996. Performance of a high-solidity Wells turbine for an OWC wave power plant. Transactions of the ASME: Journal of Energy Resources Technology 118 (4), 263–268.

Heath, T., Whittaker, T.J.T., Boake, C.B., 2000. The design, construction and operation of the LIMPET wave energy converter (Islay, Scotland). In: Proceedings of the Fourth European Wave Power Conference, Energy Centre Denmark, Danish Technological Institute, Tastrup pp. 49–55, paper B2.

Lee, C.H., Newman, J.N., Nielsen, F.G., 1996. Wave interactions with an oscillating water column. In: Proceedings of the Sixth International Offshore and Polar Engineering Conference, Los Angeles, ISOPE, I, pp. 82–90.

Pipes, L.A., Harvill, L.R., 1970. Applied Mathematics for Engineers and Physicists, 3rd ed. McGraw-Hill, Auckland.

Raghunathan, S., 1995. The Wells air turbine for wave energy conversion. Progress in Aerospace Science 31, 335–386.

Sarmento, A.J.N.A., Brito-Melo, A., 1996. An experiment-based time domain model of OWC power plants. International Journal of Offshore and Polar Engineering 6 (3), 227–233.

Sarmento, A.J.N.A., Falcão, A.F., de, O., 1985. Wave generation by an oscillating surface-pressure and its application in wave-energy extraction. Journal of Fluid Mechanics 150, 467–485.

Webster, M., Gato, L.M.C., 1999a. The effect of rotor blade sweep on the performance of the Wells turbine. International Journal of Offshore and Polar Engineering 9 (3), 233–239.

Webster, M., Gato, L.M.C., 1999b. The effect of rotor blade shape on the performance of the Wells turbine. In: Proceedings of the Ninth International Offshore and Polar Engineering Conference, Brest, ISOPE, I, pp. 169–173.